A method to obtain the wind field characteristics of super-large aperture radio telescope site based on single-point wind tower and numerical simulation

Fei-Long He[1,2], Qian Xu[2], Na Wang[2] and Chun-Hua Zhu[1]

[1] School of Physics and Technology, Xinjiang University, Urumqi 830046, China; *chunhuazhu@sina.cn*
[2] Xinjiang Astronomical Observatory, Chinese Academy of Sciences, Urumqi 830011, China; *xuqian@xao.ac.cn*

Abstract The influence of wind on the pointing accuracy of large aperture radio telescopes is becoming increasingly serious, especially at high observing frequency. Obtaining the wind field characteristics efficiently is very important to reduce the wind disturbance on antenna structure. In this paper, an error evaluation of numerical simulation method is established based on the measured data of single point wind tower, and the wind field characteristics are obtained from the evaluated numerical simulation results combined with the measured data for the 110 m aperture QiTai radio Telescope (QTT) site. According to the simulation results, compared with the measured data, the root mean square error (RMSE) of wind speed is less than $1 \, \mathrm{m \, s^{-1}}$, and the minimum wind speed RMSE is $0.2 \, \mathrm{m \, s^{-1}}$. An analysis of the wind field characteristics of the QTT site suggests that the active wind resistance design of the antenna periphery should focus on the SSW (south-south-west) direction.

Key words: telescopes — site testing — methods: data analysis

1 INTRODUCTION

In a large aperture radio telescope, coupled with the requirement of high observation frequency, the half-power beam size grows smaller, which makes the pointing accuracy more difficult to achieve. Wind disturbance has also become the most prominent natural factor affecting the pointing accuracy. In order to understand the influence of wind disturbance on antenna pointing, Smith et al. (2000) studied the dynamic characteristics of large radio telescopes in the wind on the Nobeyama Radio Observatory (NRO 45 m) telescope. The Large Millimeter Telescope (LMT 50 m) (Gawronski & Souccar 2005), the Green Bank Telescope (GBT 100 m) (Ries et al. 2011), and the Five-hundred-meter Aperture Spherical radio Telescope (FAST) (Nan 2005; Yao et al. 2017, 2020) implemented optimization measures of the control system in order to resist the effects of wind disturbance. Reviewing the upgrade process, the overall performance improvement of the control system is limited by the bottleneck of the local technology, such as compensation lag, servo error, and the increasing cost. If the interference of wind on the antenna can be weakened first, then the pressure of the antenna control system both software and hardware, to resist the wind disturbance can be effectively reduced,

and the level of extreme working wind conditions of the telescope might be further improved. Accurate wind field information is indispensable to reduce wind disturbance.

The wind field characteristics of the site can be acquired by field measurement, which is the first hand data that can be used to check the correctness of the results of different research methods. However, it is impossible to make a comprehensive measurement of the entire geographical space. The wind field characteristics of the site can be obtained by numerical simulation, whose core theory is computational fluid dynamics (CFD). The physical quantity fields of spatially and temporally continuous was discretized into a finite series of variable points, such as velocity field and pressure field. Then, based on the control equation, algebraic equations of these discrete points are established. Finally, the equations are solved to obtain approximate solutions of the flow field variables.

Under the condition that the computational amount is fine enough, the numerical simulation can simulate the fluid structure close to the real terrain and visualize the dynamic process with the help of computer graphics technology. With the improvement of computing capabilities, CFD technology has been widely developed in wind related engineering fields, such as wind farms

(Castellani et al. 2017), pollutant dispersion (Lateb et al. 2015), bridge structure (Kavrakov & Morgenthal 2018). Especially in the field of wind-resistant design of highway bridges, standard technical specifications have been formed to provide detailed guidance for wind field simulation of buildings (JTG/T 2018), and other fields are also being studied and summarized (Franke et al. 2011; Blocken 2015).

In the field of astronomy, many scholars have used numerical simulation to study the influence of wind disturbance on telescopes under different working conditions. For example, using CFD technology, Vogiatzis et al. (2014) studied the influence of performance for a large diameter optical telescope under wind loads. Mamoud et al. (2008) studied the pressure coefficient of wind load on the inner and outer surfaces of the enclosure and on the telescope primary mirror for large aperture telescope. Liu et al. (2016) studied the wind load distribution characteristics of antenna reflector structure under different windward positions, and relevant loading coefficient are obtained. This paper uses numerical simulation to study the wind field characteristics of the QTT site.

QTT will be constructed in the Qitai County of Xingjiang, China. Its working frequency is from 150 MHz to 115 GHz, and the pointing accuracy requirement is up to 2.5 arcsec (Wang 2014). Based on the universal parameter setting, the accuracy of the field characteristics obtained from numerical simulation are low. To improve the accuracy of the numerical simulation, the result can be verified by field measurements (Ha et al. 2018). The traditional verification method is to arrange wind speed sensors at multiple points in the field and compare the collected wind data with the result of the same point in numerical simulation (Blocken et al. 2015). However, astronomical telescope sites are often located in mountainous areas, far from residential areas. Usually, there are few wind data monitoring points in these areas, and the layout of wind towers is difficult. So, the traditional verification methods may not meet the requirements. To address these problems, this paper mainly studies the method of combining field measurement and numerical simulation for obtaining the wind field characteristics. This method proposes a scheme to evaluate the numerical simulation error based on the measured data of a single-point wind tower, and uses the measured data of a single-point wind tower combined with reliable numerical simulation to obtain comprehensive site wind field characteristic information.

2 MATERIALS AND METHODS

As shown in Figure 1, the QTT site is located in a basin surrounded by mountains. The basin is about 1.5 km from east to west and 2 km from north to south. The terrain is
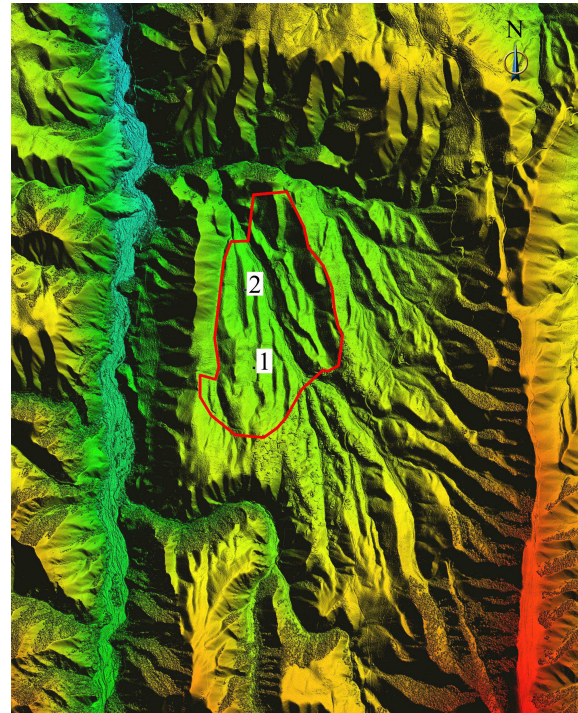

Fig. 1 QTT site. The *red line* indicates the site area, 1 and 2 stand for location of the antenna and wind tower, respectively.

high in the south and low in the north. The elevation of the mountains around the basin ranges from 1860 m to 2250 m, which has a shielding effect on the wind. To the west of the site is a long valley. The site is located in the northern foothills of the eastern section of Tianshan mountain and belongs to the temperate sub-humid mountain climate. The prevailing wind direction throughout the year is southerly wind. A 60 m height gradient wind tower was constructed at the site. The distance between the antenna site and the wind tower is about 514 m.

2.1 Verifying the Data Based on Single Point Wind Tower

The mean wind speed $V(z)$ changes with the height z above ground due to the friction between the wind and the rough elements such as grass, trees, buildings. The profile of mean wind speed is formed in the vertical plane, showing in Figure 2, which is generally described by the power law or the logarithmic law. The profile of mean wind speed of the study area can be measured through the wind tower. The error evaluation of numerical simulation is obtained through comparing with the wind profile curves measured from the wind tower. The comparison result is expressed as RMSE of two wind speed profile curves. Assuming that the RMSE are within the accuracy requirements in all major wind directions, that is, the
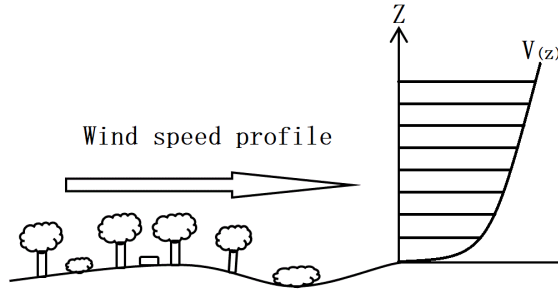
Fig. 2 Section view of the mean wind speed profile.

established numerical simulation wind field model is considered to be reliable.

2.2 Wind Tower Measured Data Processing

Starting from 5 m above the ground, a group of 2D ultrasonic sensors are equipped every 5 m, with a total of 11 layers. The sampling time of wind tower data is 1 s, collecting 1 time per minute. The 11-layer sensor generates a set of data and each layer of data contains the wind speed and direction. A set of data is generated per minute and the number of date set are 1, 2, 3 to n as shown in Table 1. The data used in this paper are from 2017 March 18 to 2017 December 31.

With the increase in height above the ground, the influence of airflow was reduced under the local terrain. The higher the wind tower, the more regionally representative the wind data are, so the wind data group of 55 m height is taken as the processing condition. Taking wind direction at 55 m height as the condition, we divide the data set according to 16 wind directions of the surface meteorological observation, shown in Figure 3, and the profile of mean wind speed at 16 directions is obtained. Wind directions at 55 m height of the tower are taken as dividing conditions of the data set, and the wind data of each layer can reflect better influence of local terrain on the mean wind profile. In the collected wind data, some of the interval wind data volume is relatively large, therefore, the method based on narrowing the range of interval was used, it can not only compress data but also reflect the trend of the whole interval. The center degree of each interval extends to the left and right of 2°, 5° and 10° respectively. Take the SSW direction as an example, 202° as the center degree, and the degree of wind direction at 55 m height represents the whole data set. According to the data shown in Table 1 (No.1~5, n), the SSW interval extends to the left and right by 2° (202°±2°) based on the middle degree, and the data set was obtained: 204, 203. Extend 5° (202°±5°) the data set are: 204, 197, 203. Extend 10° (202°±10°) the data set are: 204, 211, 197, 208, 203. Then we average the wind speed and direction of wind data at each layer
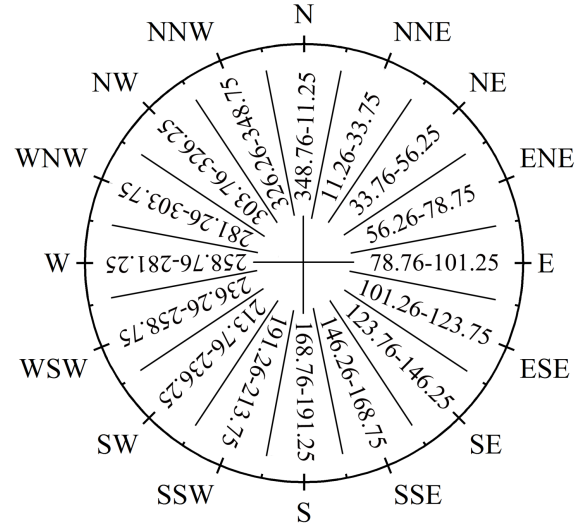

Fig. 3 Wind directions of the surface meteorological observation. Degrees (°).

of each interval. The data under multiple directions were calculated, according to Figure 4, the curve shows the same trend. Therefore, the interval size of each direction is limited to 5° to the left and right respectively.

The numerical simulation of wind field in this paper does not consider the influence of local thermal environment. However, breezes are particularly susceptible to local thermal disturbances, so data sets with low wind speeds in each wind direction should be removed. Taking wind speed at 55 m height as the processing condition, after trial calculation, it is reasonable to delete the wind data set below 5 m s^{-1}. According to this method, the wind data of each set are processed, and the mean wind speed profile curves of each wind direction in vertical space are obtained.

3 THE NUMERICAL SIMULATION

3.1 Computational Fluid Dynamics Theory

In CFD, air can be assumed as a low-speed, incompressible, viscous Newtonian fluid. We use the Reynolds Average Navier-Stokes (RANS) method for numerical simulation. This method performs time homogenization on turbulent characteristic quantities, divides instantaneous variables into average variables and pulsation variables, and uses Reynolds stress terms to represent pulsation quantities. In the wind field characteristics analysis of this paper, the thermal factor is not considered. The governing equations are as follows: Mass conservation equation

$$\frac{\partial \rho}{\partial t} + \nabla \cdot (\rho \boldsymbol{v}) = S_m. \tag{1}$$

Table 1 The Wind Tower Collecting Data

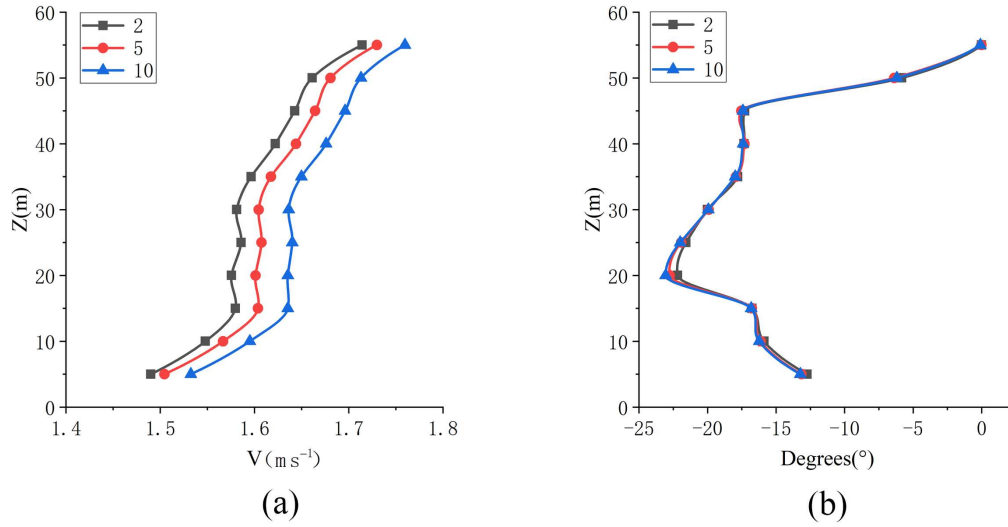|	5m speed	5m degree	10m speed	10m degree	...	50m speed	50m degree	55m speed	55m degree
1	5.19	318	6.36	318	...	5.54	330	6.32	338
2	1.00	31	1.59	122	...	7.04	197	7.37	204
3	1.02	67	2.21	162	...	6.87	206	7.02	211
4	1.59	146	2.48	157	...	6.81	188	7.54	197
5	3.14	194	5.27	209	...	6.63	202	6.23	208
⋮	⋮	⋮	⋮	⋮	⋮	⋮	⋮	⋮	⋮
n	5.08	194	5.53	191	...	8.06	201	7.70	203

Fig. 4 Three different interval ranges. The curves show the change of the speed and direction along the height. (a) Speed. The gradient curve of the average wind speed can be regarded as the wind speed profile curve in vertical space. (b) Direction.

Momentum conservation equation

$$\frac{\partial}{\partial t}(\rho \boldsymbol{v}) + \nabla \cdot (\rho \boldsymbol{v} \boldsymbol{v}) = -\nabla p + \nabla \cdot (\bar{\bar{\tau}}) + \rho \boldsymbol{g} + \boldsymbol{F}, \quad (2)$$

where ρ is the air density, $\boldsymbol{v}$ is the wind velocity vector, S_m is the source term of the mass, p is the static pressure, $\bar{\bar{\tau}}$ is the stress tensor, $\rho \boldsymbol{g}$ is the gravitational body force, and $\boldsymbol{F}$ is the external body force.

Based on CFD theory, several software packages were developed. For this paper, we use Fluent software which is a popular working platform. There are a variety of turbulence models available in Fluent, such as Standard $k - \varepsilon$ model, RNG $k - \varepsilon$ model, Realizable $k - \varepsilon$ model, etc. We adopt the Realizable $k - \varepsilon$ model, which is newer and has higher precision (Li et al. 2011).

3.2 Geographic Model

The geographical model with the wind tower and antenna as the target area was used to determine a central point in the site and establish a core area with a diameter of 1 km and then extended around. According to the preliminary investigation, this paper is concerned about the incoming wind in the positive direction and its adjacent directions. The simulation is modeled with 12 directions as shown in Figure 5. The wind directions are defined based on 16 wind directions of the surface meteorological observation. For the incoming wind direction, taking the south direction as an example, SSW, S and SSE direction belong to the south direction. The geographic data come from the ASTER GDEM data downloading from Geo-Cloud Space (*http://www.gscloud.cn*), which is jointly developed by Japan METI and NASA USA and release to the public free. Considering that the mountainous terrain is more complicated, the mesh is divided by an adaptive non-structural mesh. The boundary layer is set up along the ground with an initial height of 5 m, set to eight layers, and a total height is 80 m.

3.3 Boundary Conditions

The inlet profile of mean wind speed of calculation domain uses the power law, as follows:

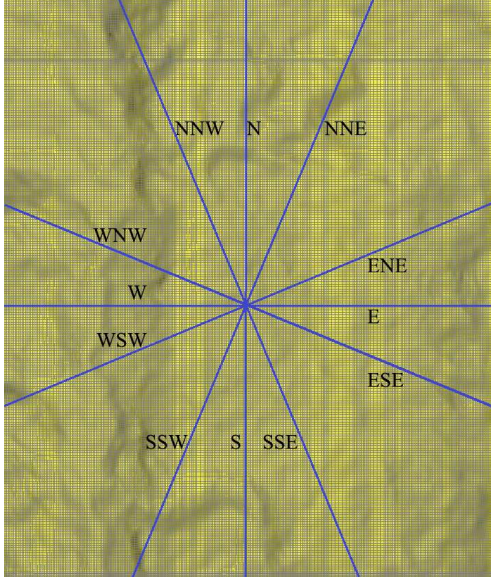$$V(z) = V_0 \left(\frac{z}{z_0}\right)^{\alpha}. \quad (3)$$
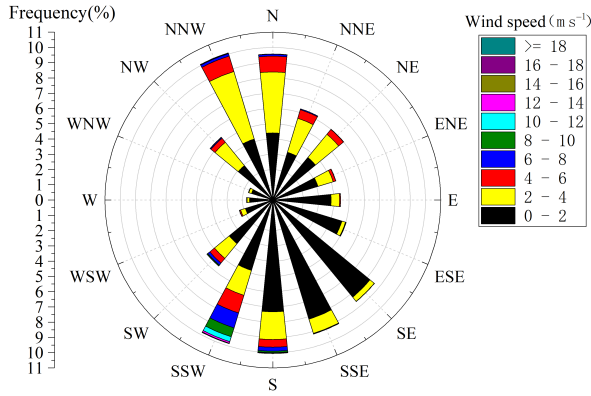
Fig. 5 Numerical simulation map.

Fig. 6 Wind rose diagram. The wind rose diagram is produced from wind data at a height of 55 m.

According to the actual terrain of the site, it belongs to class B, and the α index is 0.15. We use $z_0 = 10$ m, which is recommended by the specification. According to the analysis and processing of the measured data, we set $V_0 = 5$ m s^{-1}.

The intensity of incoming turbulence is based on type 2 of landforms in the Japanese specification.

$$I(z) = \begin{cases} 0.23, & z \leq 5 \\ 0.1(\frac{z}{z_g})^{-0.2}, & 5 < z \leq z_g \end{cases} \quad (4)$$

where z_g is 350 m.

The empirical formula of turbulence integral scale is given by

$$L_u(z) = \begin{cases} 100, & z < 30 \\ 100(\frac{z}{30})^{0.5}, & z \geq 30 \end{cases}. \quad (5)$$

The above boundary conditions can be implemented in the Fluent software through the user-defined function (UDF).
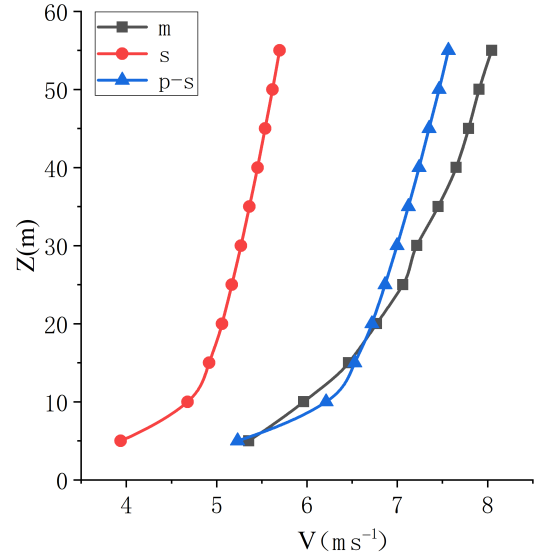

Fig. 7 Normalization of both data. m represents measured data, s represents simulation data and $p - s$ represents simulation after processing data.

4 EVALUATION OF NUMERICAL SIMULATION RESULTS BASED ON MEASURED DATA

We process the wind data of 55 m from the wind tower into the wind rose diagram in Figure 6. From the perspective of wind frequency, the wind is mainly in the north-south direction and less in the east-west direction. In the north direction, the wind frequency of NNW and N direction is higher; in the south direction, the wind frequency of all directions is generally higher. From the perspective of wind speed, the speed of wind coming from all directions is mostly below 4 m s^{-1}. Except for the SSW direction, the wind speed in all directions is generally lower than 10 m s^{-1}. Combined with the topography shown as in Figure 1, the analysis is as follows. The NNW and N direction in the north are just at the mouth of the canyon, so the frequency of incoming wind is high. For the south direction, there are no vertical wind direction's mountains in the upwind mouth, so the effect of blocking wind load is weak. The SSW direction is just located in the mountain gap, which is west of antenna. The strong wind from the snow mountain can blow to the site area, the wind of speed and frequency in this direction is relatively high.

4.1 Normalization of Numerical Simulation Results with Field Measured Data

In the simulation, the initial velocity of the wind field inlet is based on the average wind speed setting of the whole area, this is different from the actual inlet wind speed. This leads to a certain difference of reference speed V_0 of wind speed profile curve between the simulated

and measured, as show in Figure 7. Therefore, this paper proposes to multiply the simulation result by a scale factor a to normalize the reference speeds of the simulated and measured.

First, we fit the measured and simulated scatter data to wind speed profile curves and then obtain speed constant c and index α respectively.

$$y_m = c_m x^{\alpha_m}, \qquad (6)$$

$$y_s = c_s x^{\alpha_s}. \qquad (7)$$

m represents actual measurement, s represents simulation, x is the height, and y is the wind speed.

According to the wind speed profile Equation (3), the derivation process is as follows

$$V_m = V_{m_0}(\frac{z}{z_0})^{\alpha_m} = V_{m_0}(\frac{1}{z_0})^{\alpha_m} z^{\alpha_m} = c_m x^{\alpha_m}, \quad (8)$$

$$V_s = V_{s_0}(\frac{z}{z_0})^{\alpha_s} = V_{s_0}(\frac{1}{z_0})^{\alpha_s} z^{\alpha_s} = c_s x^{\alpha_s}. \quad (9)$$

Replacing V_{s_0} in Equation (9) with V_{m_0} in Equation (8) to normalize, it is equivalent to the same reference speed for simulation and measurement, hence we get the formula:

$$V_s^p = \frac{c_m(\frac{1}{z_o})^{\alpha_s}}{c_s(\frac{1}{z_o})^{\alpha_m}} V_s . \qquad (10)$$

The scale factor a is:

$$a = \frac{c_m(\frac{1}{z_o})^{\alpha_s}}{c_s(\frac{1}{z_o})^{\alpha_m}} . \qquad (11)$$

4.2 Comparison between Simulation and Actual Measurement

In the numerical simulation results, the data at the same location as the measured points were extracted and normalized according to the method in Section 4.1 to obtain the simulated and measured wind speed profile curves under each wind direction, see Figure 8. The wind frequency of after processing and the RMSE of simulation and measurement are statistical under each wind direction, as shown in Table 2.

According to Figure 8, it can be seen that the wind speed profile curve obtained by simulation is consistent with the overall trend compared with the measured one. In the north direction and the south direction, the two curves are in good agreement, while in the west direction, the simulation is in weak agreement with the actual measurement. According to Table 2, the wind speed RMSE of both the measured and simulated curves is less than 1 m s^{-1}. The directions of wind speed RMSE less than 0.5 m s^{-1} are account for $\frac{2}{3}$, and the minimum wind speed RMSE is 0.2 m s^{-1}. We analyze the reasons for the

directions of wind speed RMSE bigger than 0.5 m s^{-1}. (1) In these directions, the original wind collected by the wind tower has less frequency, and the amount of data is less after processing (Table 2). It has a large random error in data statistics. (2) According to Figure 1 and Figure 6, we can see that for the wind in the WSW, W and WNW direction, the mountain is located just upstream of the wind tower; for the incoming wind in the E direction, the mountain is located just downstream of the wind tower. The incoming winds in these directions will be strongly disturbed by mountain, which will increase the degree of turbulence of air flow, so the accuracy of measurement and simulation will be affected. Under the same mesh density, the accuracy of numerical simulation results will be reduced. A more accurate simulation requires finer meshes and multiple calculations. Considering that the wind frequency from these directions is not high and the wind speed is not large, further calculation is not significant.
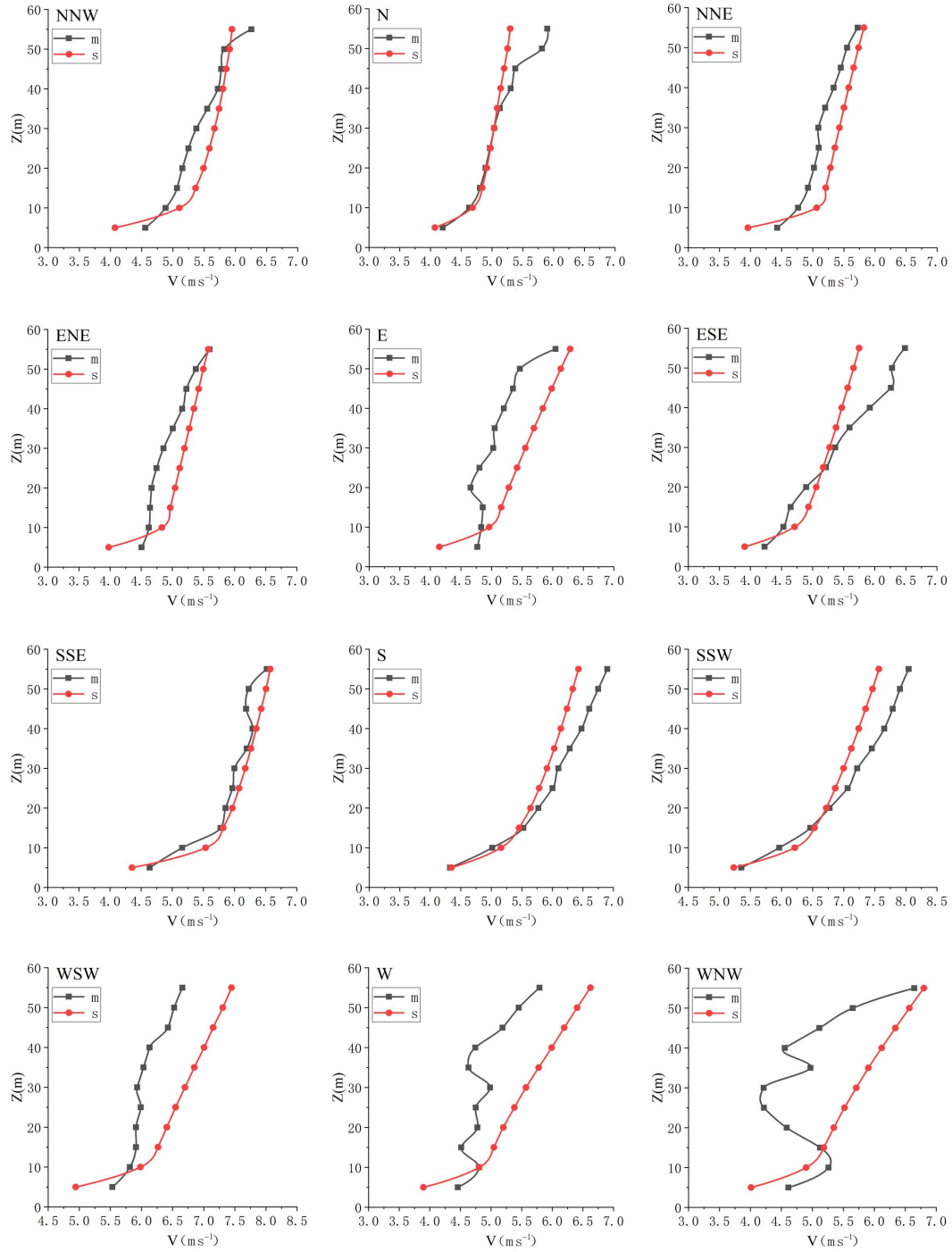
5 ANALYSIS OF THE WIND FIELD CHARACTERISTICS AT THE QTT SITE

According to the numerical simulation results, the wind data for elevation of 55 m relative to the ground is extracted to create the vector diagram of the wind speed distribution. Figure 9 shows the speed distribution and flow direction of incoming wind in different directions. We found that the wind is significantly weakened by the influence of terrain at a height of 55 m, and the airflow tends to be basically stable, with no obvious large airflow disturbance and deflection. Incoming winds from the north and south have relatively small distribution differences of wind speed within the site area; for incoming winds from east and west, the speed distribution differences within the site area are relatively large. Especially in E, ESE and W direction, the antenna position is close to the wind acceleration zone, and the wind field formed is relatively unstable. In general, local representative wind data of the target area can be measured by field measurement, and more detailed information can be obtained by combining with numerical simulation. In $\frac{2}{3}$ directions of them, such as NNE, ESE, SSW, etc, the wind speed in the antenna area is greater than that in the wind tower. In the other directions, the wind speeds at the two points are almost equal.

Analysis based on Figure 1, Figure 6 and Figure 9, suggest as follows. (1) Active wind resistant design around the antenna in the future, such as setting up wind-proof nets, wind-proof walls, forest belts, etc, are mainly in the SSW direction. According to Figure 6, we can find that the wind frequency reaches about 10% in SSW direction and the wind speeds greater than 6 m s^{-1}, about 2%, are mainly in this direction. If the problem of wind

Table 2 The Wind Frequency and the RMSE

Directions	NNW	N	NNE	ENE	E	ESE	SSE	S	SSW	WSW	W	WNW
Frequency	1278	875	361	102	37	38	23	1045	6949	67	20	17
RMSE (m s^{-1})	0.28	0.26	0.28	0.30	0.54	0.42	0.20	0.28	0.31	0.66	0.80	0.99

Fig. 8 Wind speed profile curves of simulation and actual measurement at each wind direction. m represents measured data and s represents simulation data.
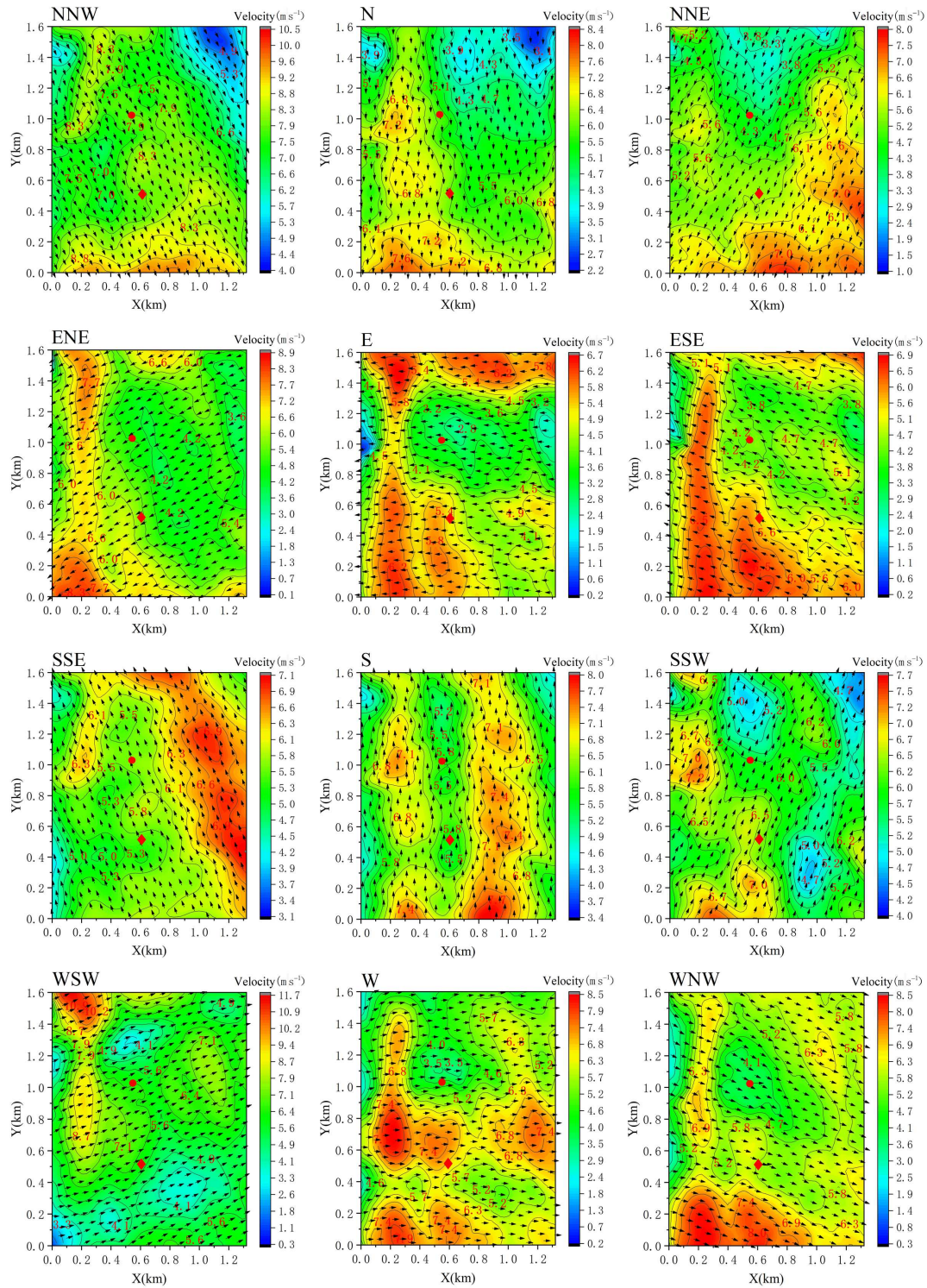
Fig. 9 Vector diagram of the wind speed distribution at height of 55 m relative to the ground. The different colors indicate the wind speed gradient, and the arrows represent the direction of the wind, ♦ antenna, • wind tower, and X, Y are distance.

disturbance in this direction can be effectively solved, then the observation time of the telescope will be effectively increased. (2) Although the wind speed from the north is low, the wind frequency from the mouth of the canyon is high, which reaches 20%. From the physiographical point of view, the width of the mouth of the canyon is

relatively small. It is about 550 m, and the raised peaks in the valley facilitate the construction of windbreaks. If active wind resistance operation is carried out first from here, the engineering quantity is small and it is relatively simple to deal with, which can provide experience for anti-wind operation in other directions.

6 CONCLUSIONS

This paper mainly discusses the method of evaluating the error of numerical simulation with the measured data of single point wind tower. Based on the field measured and numerical simulation, the basic wind field characteristics of the QTT site were obtained, and the wind field characteristics were quantitatively analyzed.

The error of numerical simulation is evaluated by the measured data of single-point wind tower, according to the comparison results, both trends of the wind speed profile curve are consistent and the RMSE of the wind speed is less than $1\,\mathrm{m\,s^{-1}}$. The directions of wind speed RMSE less than $0.5\,\mathrm{m\,s^{-1}}$ accounts for $\frac{2}{3}$, and the minimum wind speed RMSE is $0.2\,\mathrm{m\,s^{-1}}$. Therefore, the established numerical model is relatively reliable.

According to the measured data, the main wind is in the north and south direction of QTT site. In all directions, 90% of the incoming wind are below $4\,\mathrm{m\,s^{-1}}$. According to the numerical simulation results, the airflow tends to be basically stable at 55 m, with almost no extreme wind conditions. In the future, the active wind resistance design of QTT periphery should focus on the SSW direction, and the project of wind resistance can be carried out from the mouth of the canyon first.

Through numerical simulation, a reliable site wind field structure could be obtained, and the reference wind resistant areas could be found using wind streamline. Only setting a small quantity of shelters, such as tall tree, windproof net, and so on can change the wind flow direction, which would reduce the wind's power at the antenna position, the telescope's effective observation time would be improved. The effect of the selected resistant areas can be set in the simulation to conduct verification.

References

Blocken, B. 2015, Builing and Environment, 2015, 1, *http://dx.doi.org/10.1016/j.buildenv.2015.02.015*

Blocken, B., van der Hout, A. , Dekker, J., & Weiler, O. 2015, Journal of Wind Engineering and Industrial Aerodynamics, 147, 43

Castellani, F., Astolfi, D., Mana, M., et al. 2017, Wind Energy, 20, 1277

Franke, J., Hellsten, A., Schlünzen, K. H., & Carissimo, B. 2011, International Journal of Environment and Pollution, 44, 419

Gawronski, W., & Souccar, K. 2005, Antennas and Propagation Magazine, 47, 41

Ha, T., Lee, I.-B., Kwon, K.-S., & Lee, S.-J. 2018, Computers and Electronics in Agriculture, 149, 110

JTG/T 3360-01-2018. 2018, Wind-resistant Design Specification for Highway Bridges, China

Kavrakov, I. & Morgenthal, G. 2018, Journal of Fluids and Structures, 82, 59

Lateb, M., Meroney, R. N., Yataghene, M., et al. 2015, Environmental Pollution, 2015, 1, *http://dx.doi.org/10.1016/j.envpol.2015.07.039*

Li, P.-F., Xu, M.-Y., & Wang, F.-F. 2011, Fluent Gambit Icem Cfd Tecplot (1st ed.; Beijing: Post & Telecom Press) (in Chinese)

Liu, Y., Qian, H.-L., & Fan, F. 2016, Advanced Steel Construction, 12, 380

Mahmoud, M., Tahi, A., Benmeddour, A., et al. 2008, Journal of Wind Engineering and Industrial Aerodynamics, 96, 257

Nan, R.-D. 2005, Science In China Ser. G Physics, Mechanics & Astronomy, 35, 449 (in Chinese)

Ries, P., Hunter, T. R., Constantikes, K. T., et al. 2011, PASP, 123, 682

Smith, D. R., Paglione, T. A. D., Lovell, A. J., Ukita, N., & Matsuo, H. 2000, in Proc. SPIE, 4015, Astronomical Telescopes and Instrumentation, ed., H. R. Butcher, 467

Vogiatzis, K., Segurson, A., & Angeli, G. Z. 2004, in Proc. SPIE, 5497, Modeling and Systems Engineering for Astronomy, ed., S. C. Craig, M. J. Cullum, 311

Wang, N. 2014, Scientia Sinica Physica, Mechanica & Astronomica, 44, 783

Yao, R., Li, Q.-W., Sun, J.-H., Sun, C.-H., & Zhu, W.-B. 2017, Journal of Mechanical Engineering, 53, 36 (in Chinese)

Yao, R., Jiang, P., Sun, J.-H., Yu, D.-J., & Sun, C. 2020, RAA (Research in Astronomy and Astrophysics), 20, 68